
Article:
Ballard, DA orcid.org/0000-0002-5506-199X, Qiao, P, Cattoz, B orcid.org/0000-0003-3123-0936 et al. (7 more authors) (2020) Aggregation Behavior of E-SARA Asphaltene Fractions Studied by Small-Angle Neutron Scattering. Energy & Fuels, 34 (6). pp. 6894-6903. ISSN 0887-0624

https://doi.org/10.1021/acs.energyfuels.0c00596

Aggregation Behaviour of E-SARA Asphaltene Fractions Studied by Small-angle Neutron Scattering

Ballard, D. A.[1], Qiao, P.[2], Cattoz, B.[4], Dowding, P. J.[4], Prevost, S.[3], Alshamsi, M.[1], Charpentier, T.[1], Roberts, K. J.[1], Xu, Z.[2], Harbottle, D.[1*]

1) School of Chemical and Process Engineering, University of Leeds, Leeds, UK.

2) Department of Chemical and Materials Engineering, University of Alberta, Edmonton, Canada.

3) Institut Laue-Langevin, 71 avenue des Martyrs, CS 20156, 38042 Grenoble cedex 9, France.

4) Infineum UK Ltd., Abingdon, Oxfordshire, UK.

ABSTRACT

Using the Extended-SARA method to fractionate asphaltenes based on their interfacial activity, the current study reports the first results on the estimated size and shape of interfacially active (IAA) and remaining (RA) asphaltene nanoaggregates. These fractions have been reported to exhibit distinctly different chemical architectures that influence the size of asphaltene clusters in good and poor solvents. However, little is known about the building blocks, commonly referred to as nanoaggregates, which form these clusters and how those subtle differences in chemical architecture impact aggregation of asphaltenes. The nanoaggregate size and shape of IAA and RA was measured using small-angle neutron scattering (SANS). The characteristic length and asymptotic power-law exponent of whole asphaltenes (WA) extracted from heavy crude oil and dispersed in deuterated toluene were 28.0 Å $\pm$ 0.2 Å and 2.86 $\pm$ 0.01, respectively, showing negligible variations with changing asphaltene concentration, source of asphaltenes (bitumen and heavy crude oil), and solvent aromaticity. For RA fractions, which account for 98.5 wt% of WA, the characteristic length and power-law exponent of 28.8 Å and 2.86 were comparable to that of WA, but in contrast to 59.7 Å and 2.20 for IAA. A ~100% increase in the characteristic length and reduced power-law exponent of the IAA fraction confirms that these two asphaltene sub-fractions form dissimilar nanoaggregate structures.

INTRODUCTION

Asphaltenes are commonly described as the heaviest fraction in crude oil and are soluble in aromatic solvents and insoluble in n-alkanes. In the production of crude oil, asphaltenes can be problematic due to their propensity to adsorb at oil-water and solid-oil interfaces, forming asphaltene and/or particle films that stabilize water-in-oil (W/O) emulsions,[1-3] as well as fouling of surfaces,[4, 5] leading to problems in fluid flow and heat transfer. Due to their problematic nature, significant research to characterize asphaltenes and correlate asphaltenes physicochemical properties to their behaviour has been undertaken. It is generally accepted that asphaltenes are polycyclic molecules containing ~7 aromatic rings with protruding aliphatic side chains,[6, 7] with molecular weight of ~750 Da.[6, 8] Asphaltenes are considered the most polarizable fraction of crude oil due to the presence of heteroatoms such as oxygen, sulfur and nitrogen which can be found in both the aromatic cores and aliphatic side chains.[7, 9]

While most research has considered the behavior of whole asphaltenes (WA), several recent studies have considered isolating the interfacial material. Fractionation methods have included the use of D_2O-oil and H_2O-oil emulsions,[2, 10-12] and adsorption on particles.[13-16] Although different extraction methods have been adopted, characterization of the interfacial material reveals a consistent understanding, that is, the interfacial material is enriched in O_x and O_xS_y containing species and higher carboxylic functionalities. Xu et al. proposed the Extended-SARA (E-SARA) method to isolate asphaltenes partitioned at an oil-water interface from those remaining in the bulk solvent,[12, 17] with the two fractions named 'interfacially active asphaltenes' (IAA) and 'remaining asphaltenes' (RA). A series of studies focused on characterizing the physicochemical properties of these two asphaltene sub-fractions and provided an understanding of the chemical architecture of IAA and RA and the prominent functional groups in the IAA fraction.[12, 17-20] The IAA fraction was found to be ~2 wt% of WA and characterized by high oxygen and sulfur species, with the increased oxygen content believed to be associated with sulfoxide groups,[18] which were shown to contribute to the strong aggregation of IAA molecules relative to RA molecules.

Depending on the fluid properties (aromaticity, temperature and pressure), asphaltenes aggregate to form large clusters via a size hierarchy typically described by asphaltene molecules (Å), nanoaggregates (nm) and clusters (nm to μm). The mechanism for asphaltene aggregation to various scales is debated by the Yen-Mullins[21] and supramolecular[22] structural models. The Yen-Mullins model describes aggregate growth via π-π interactions between

aromatic cores with steric hindrance from aliphatic side chains limiting the size of asphaltene aggregates. Following the prominent study of Agrawala and Yarranton, where it was postulated that asphaltenes self-associate by a linear polymerization mechanism,[23] Gray et al. proposed a supramolecular growth model that includes other possible interactions between asphaltenes such as i) π-π stacking, ii) hydrogen bonding, iii) van der Waals forces and iv) acid-base interactions.[22] The supramolecular model suggests the interactions of asphaltene molecules, through multiple intermolecular forces, forms large nanoaggregates/clusters of varying size and shape.

Asphaltene nanoaggregates have been resolved by small-angle neutron scattering (SANS). SANS data represents the radial average of the scattering intensity, also known as the scattering cross section, and represents a volume-weighted average of the scattering material. The scattering cross section ($d\Sigma(Q)/d\Omega$) is plotted against the scattering vector, Q ($Å^{-1}$), which is related to the length (diameter, D) of the scattering material by $Q = 2\pi/D$. Shape-independent and -dependent models are calculated for theoretical sizes and shapes, and fitted to the scattering profile to determine the original properties of the scattering material. The gradient of the profile gives structural information, while the asymptotic behavior of the Q value determines the radius of gyration, R_g.

While experimental data is rather featureless and reflects the diverse nanoaggregate structures, common shape-dependent models used to fit SANS data include i) mono- and poly-disperse spheres,[24, 25] ii) thin disks,[25, 26] iii) spherical micelles,[27] iv) prolate ellipsoids,[28] v) oblate cylinders[29] and vi) hollow spherical vesicles.[30] While the range of reported structures may be attributed to different sources of asphaltenes, caution should be given to the method and hypotheses used for structure determination. The possibility of physically unreasonable fittings to the SANS data can arise from a high number of tuneable fitting parameters which may distort the true significance of the data. This is especially true for models with a high number of tuneable parameters which force uniformity in asphaltenes structures. The goodness of fit is typically reported by a χ^2 value which evaluates the degree of uncertainty between theoretical and experimental data. While χ^2 values between < 1.0 and ~400 have been reported,[25, 28, 29, 31] lower values provide greater confidence in the model fitting. It is worth noting that SANS/SAXS techniques are only suitable to provide meaningful bulk characteristics rather than discrete characteristics, hence fractionation methods are a viable route to observe differences in bulk characteristics. Similar asphaltenes fractions studied by mass spectrometry

revealed the polydisperse nature of asphaltenes as strong solute-solvent interactions prevented ionization of *archipelago-like* structures, leading to a bias in previous literature towards *island-like* molecular structures.[22, 32] Differences in solute-solvent interactions between asphaltene molecular structures, emphasises that no well-defined phase stability envelope exists and small amounts of asphaltenes precipitate even at dilute conditions,[33] a result of asphaltenes exhibiting significant differences in their relative solubility.[34, 35]

Asphaltene nanoaggregates typically exhibit a radius of gyration (R_g) in the order of several nanometres.[28, 31, 33, 36] The fitting of shape-independent models to asphaltenes SANS data has been widely used and reported in literature.[31, 37-39] Many shape-independent models (Guinier-Porod, Beaucage, Zimm) infer an asphaltene nanoaggregate size (R_g) between 15 and 50 Å,[31, 36, 39] and a Porod exponent between 2 and 2.5[37-39] in pure solvents or native crude oils. The asymptotic behavior of intensity at high-Q follows a power-law decay ($I(Q) \sim a \times Q^{-b}$), where the coefficient b is termed the Porod exponent and takes the value of 4 for scatterers of any shape with a sharp interface, a value between 3 and 4 for surface fractals and a value between 1 and 3 for mass fractals, where the fractal dimension is approximated by the Porod exponent. More compact structures exhibit a Porod exponent closer to 3. A Porod exponent of 2 can result from highly fluctuating clusters with ill-defined shape such as those observed when coming close to a critical point.[40] Note that the mass fractal model with D_f = 2 to 2.5 (Porod exponent = 2 to 2.5) is consistent with viscometric data,[37] with the measurement of intrinsic viscosity also used to interpret size and structural features of asphaltenes aggregates.[41]

Solution properties associated with the aggregation of asphaltenes such as asphaltene concentration, solvent aromaticity and solvent addition procedure have been shown to affect the structure of nanoaggregates but more strongly the size of larger asphaltene clusters.[35, 39, 41, 42] Roux et al.[39] studied the effect of asphaltene concentration and showed a decrease in R_g by ~40% with increasing asphaltene concentration from ca. 4 – 10 vol%, with the nanoaggregate size, R_g ~70 Å at 20˚C, independent of asphaltene concentration between ~0.3 and 4 vol%. This is reasonable since the asphaltene concentration greatly exceeded the critical nanoaggregate concentration (CNAC), with values often reported in the region of 0.1 g/L (~0.01 vol%).[3, 43] Increasing solvent temperature has been shown to decrease the size of nanoaggregates in pure solvents and real crude oils, with the temperature-dependence on nanoaggregate size being more sensitive to temperature changes around ambient temperature.[31, 39, 44] When decreasing

solvent quality (reduced aromaticity through the addition of n-alkanes), Yang et al. found that solvent quality did not affect the size of nanoaggregates but affected the structure of larger clusters.[42] Comparing four asphaltene samples, Spiecker et al.[35] showed a size increase of nanoaggregates towards the solubility limit. The size of the most soluble asphaltene (AH) was weakly dependent on solvent aromaticity and the authors attributed the solvent dependency for each asphaltene sample to the asphaltene H/C ratio and nitrogen content, with a low H/C ratio corresponding to the least stable asphaltenes.

Shape-dependent models have also been used to determine the size of asphaltene nanoaggregates, with a Schulz distribution often leading to lower χ^2 values than Gaussian or monodisperse systems.[24, 29, 31] There are often few notable structural features for asphaltenes which limits the confidence of selecting suitable shape-dependent models, as featureless profiles are indicative of systems of polydisperse nature.[31] Eyssautier et al.[25] compared both sphere and cylinder models for the same asphaltenes in toluene, and showed the best fit (χ^2 = 188) to a disk-like core-shell cylinder model with dimensions of 7 Å height and 33 Å radius. In contrast, fitting a spherical model led to a radius of 29.8 Å and χ^2 of 1125. Shape-independent models, although providing less structural information, provide more consistent geometrical parameters than shape-dependent models, particularly for complex systems where structure is poorly defined and the sample is polydisperse.

Large asphaltene clusters have been measured using small-angle scattering (SAS). However, the size of asphaltene clusters is not typically reported due to limited resolution in the low-Q range. Headen et al.[31] studied asphaltenes by very small-angle neutron scattering (V-SANS) with Q-values as low as 2×10^{-4} Å^{-1}, and commented on the coexistence and independence of asphaltene nanoaggregates and clusters, since fitting the Beaucage model, a model that describes the formation of larger structures from discrete smaller structures, did not provide a good fit to the scattering intensity profile. Similarly, Hoepfner et al.[33] suggested that asphaltene solutions contain both stable and unstable asphaltene nanoaggregates, with unstable nanoaggregates forming the large clusters. These stable nanoaggregates were observed at asphaltene concentrations as low as 15 mg/L.[8]

While most SAS studies characterize asphaltenes in bulk solvent, Jestin et al.[45] characterized the scattering contribution from asphaltenes stabilizing water-in-oil emulsions (interfacial asphaltenes). The authors compared the size of asphaltenes in the bulk solvent prior to and

following emulsification and showed a decrease in size of asphaltenes remaining in the solvent by ~7.5 to 15%, with the size change dependent on the resins content. It appeared the larger asphaltene aggregates preferentially adsorb at the water-oil interface. Reducing the form factor to a simple geometric model of large flat disks, the characteristic length of the interfacial film was found to be ~130 Å and scaled approximately with twice the radius of gyration of asphaltene nanoaggregates in solution, suggesting the stabilizing interfacial layer was one monolayer of nanoaggregate thick.

Given the limited characterization of asphaltenes partitioned at an oil-water interface, the current study aims to compare the size and shape of WA extracted from a heavy crude oil and bitumen, and then adopts the E-SARA method to compare IAA and RA fractions (extracted from heavy crude oil) re-dispersed in d-toluene. The study was designed to assess whether differences in physicochemical properties of asphaltenes affect the structure of asphaltene nanoaggregates.

MATERIALS AND METHODS

Heavy crude oil and bitumen with an API of 13.6° and < 10° (at 60 °F) were sourced from the Llanos region in Colombia and Athabascan region in Canada, respectively. Whole asphaltenes (WA) was extracted from bitumen and heavy crude oil using the precipitation and wash method previously described.[20] The E-SARA method described by Yang et al.[12] was followed to separate WA into remaining asphaltenes (RA) and interfacially active asphaltenes (IAA) fractions. Briefly, the method involved dispersing 10 mL of deionized water in 100 mL of 10 g/L WA-in-toluene using a homogenizer (T18 Ultra-Turrax, IKA, UK) at 13,000 rpm for 15 min. The emulsion was left to gently agitate for 24 h before centrifuging the emulsion at 11,000 rpm (Heraeus Megafuge 16 Centrifuge, ThermoFisher Scientific, UK) to separate the stable water droplets from the continuous oil phase. The supernatant was then removed without disturbing the emulsion-cake and fresh toluene added and shaken to remove any loosely bound asphaltenes at the water-oil interface. Following 6 consecutive toluene washes, the emulsion droplets were transferred to a pre-weighed glass beaker and left for 12 h in a vacuum oven at 60°C for the deionized water and any remaining solvent to evaporate. From 1 g of WA heavy crude (asphaltene content of the heavy crude oil was ~25 wt%), approximately 15 mg of IAA was obtained, confirming that the fraction of asphaltenes partitioned at the oil-water interface

was ~1.5 wt% of WA. HPLC grade toluene and heptane along with deuterated equivalents were supplied by Sigma-Aldrich.

Elemental Analysis: An EA112 Flash Analyzer (CHNS/O) was used to determine the elemental composition of WA, RA and IAA obtained from heavy crude oil and WA from bitumen. According to the standard method recommended by the instrument manufacturer, 2 mg of each fraction was analysed, with the mass range found to have no effect on the sample composition. The results reported were the average of four independent runs to minimise sampling and analysis error.

Fourier Transform Infrared Spectroscopy (FTIR): FTIR spectra of the heavy crude oil asphaltene fractions were obtained using a Nicolet iS10 FT-IR Spectrometer (Thermo Scientific) equipped with an attenuated total reflection (ATR) sampling accessory in the spectral range between 4000 and 500 cm^{-1} at a spectral resolution of 2 cm^{-1}. A single spectrum was collected from a total of 32 scans. For semi-quantitative analysis, all FTIR spectra were normalized with respect to the strongest adsorption peak of the aliphatic C−H stretching vibrations between 2780 and 3000 cm^{-1}.

Nanostructure-assisted laser desorption/ionisation (NALDI): Experiments were performed on an ultrafleXtreme™ MALDI-TOF/TOF (Bruker Daltonics, Billerica, MA, USA) mass spectrometer in positive MS mode at m/z ratio from 120 to 2000. Asphaltene samples were dissolved at a concentration of 50 g/L in toluene, sonicated for 10 min and used immediately. 1 µL of sample solution was spotted to a Bruker NALDI™ target (nanostructured laser desorption ionization target, Bruker Daltonics, Billerica, MA, USA) and dried prior to analysis. Data was processed and analysed by FlexControl and FlexAnalysis software (Bruker Daltonics, Billerica, MA, USA).

Small-Angle Neutron Scattering (SANS): SANS experiments were conducted using beamline D33 at the Institut Laue-Langevin (ILL), Grenoble. Samples of 5 mL asphaltene solutions were prepared either in 5 g/L toluene-d8 99 atom% D, or 3:2 volume ratio of heptane-d16:toluene-d8 99 atom% D mixtures (d-heptol). The prepared solutions were tip sonicated (Q500 Sonicator, Fisher Scientific) for 2 min before pipetting 250 µL of the prepared asphaltene solution into 280 µL cylindrical quartz cells (Type 120-QS, Hellma). All scattering experiments were conducted at 24.5°C. Three configurations were used, with sample-to-

detector distances of 2, 10 and 12 m, and wavelengths (λ) of 4.6, 4.6 and 13 Å, respectively (relative FWHM 10 %). Additionally, 4 detector banks were used at 1.2 m to cover the high-Q range, thus covering a scattering angle (θ) range of 0.12° – 21°. Data from the 3 configurations are represented by blue (~0.04 to 0.5 $Å^{-1}$), black (~0.005 to 0.05 $Å^{-1}$) and red (~0.001 to 0.01 $Å^{-1}$) symbols in the figures. The overall Q-range was 0.001 – 0.5 $Å^{-1}$, where Q is the scattering wavevector of magnitude, which is inversely proportional to the length-scale probed:[46]

$$Q = 4\pi\lambda^{-1} sin\,(\theta/2) \qquad \text{Eq. 1}$$

The collection time for the three configurations was set to 60 s, 300 s and 1800 s, respectively. Samples were measured several times over a period of 6 h with no significant differences between data, thus the data was consequently averaged.

SANS Data Analysis: According to scattering theory, the scattering cross section, dΣ(Q)/dΩ, from a scattering material is given by:[46]

$$\frac{d\Sigma(Q)}{d\Omega} = \Phi\Delta\rho^2 {V_A}^2 P(Q)S(Q) \qquad \text{Eq. 2}$$

where Φ is the particle volume fraction, $\Delta\rho^2$ the contrast factor and V_A the aggregate volume. *P(Q)* is the form factor and provides information for size and shape, while *S(Q)* is the structure factor and provides information on inter-particle interactions. The contrast factor is the square of the difference in scattering length density (SLD, commonly denoted as ρ) between the solvent and asphaltene nanoaggregates and was determined experimentally by adjusting the SLD of the solvent, as shown in the Supplementary Information A1.

Measured scattering intensities were normalized to an absolute scale. Data reduction of the SANS data was performed using LAMP (software provided by ILL). SasView[47] was used to fit the scattering profiles using the Levenberg-Marquardt algorithm,[48] which is commonly used for fitting of non-linear least square problems. A shape-independent empirical model commonly referred to as the Broad Peak model was fitted to all scattering data fixing the peak position at Q = 0 $Å^{-1}$. A broad Lorentzian-type peak was fitted on top of a power law decay to give a characteristic length for the nanoaggregates and a measure of shape and volume. This approach was chosen as shape-independent models are less likely to lead to unrealistic

representations of the scattering sample due to the lower number of tuneable parameters that reduce the possibility of physically unreasonable models, especially in systems where structures are ill-defined.[49] The scattering intensity, I(Q), is fitted by:

$$I(Q) = \frac{A}{Q^n} + \frac{C}{1+ (|Q-Q_0|.\xi)^m} + B \qquad \text{Eq. 3}$$

where A is the Porod law scale factor, n the Porod exponent, fixed to $n = 4$ based on initial fitting results, C the Lorentzian scale parameter which leads to the extrapolated scattering intensity at $Q = 0$, ξ the characteristic length of the nanoaggregates, m the exponent of the Lorentzian function which can be considered to be the fractal dimension of the nanoaggregates, and B is a constant that accounts for incoherent scattering from hydrogen, but also contains other contributions that are Q-independent in the probed range. The value B resulting from the fit is subtracted from intensity data. The Broad Peak model was fitted across the whole Q-range collected for all samples, with the peak position (Q_0) fixed at 0 Å^{-1}. For samples which exhibited weak scattering in the low-Q region (~0.001 to 0.01 Å^{-1}), two fits of the data were made which included and excluded the low-Q region scattering.

The Lorentzian scale parameter provides the scattered intensity at $Q = 0$ Å^{-1}, determined by fitting the high-Q data. Then the volume of the asphaltene nanoaggregates can be approximated by:

$$I(0) \approx \Phi V \Delta\rho^2 \qquad \text{Eq. 4}$$

where Φ is the volume fraction (~0.005), V the nanoaggregate volume (Å^3), and $\Delta\rho^2$ the contrast, which is the difference in square of scattering length density, ρ, between the asphaltenes and solvent (Å^{-2}).

RESULTS AND DISCUSSION

Asphaltene Characterization

The elemental compositions of WA, RA and IAA extracted from heavy crude oil and WA from bitumen are shown in Table 1. Similar to previous characterizations of different oil samples, IAA is slightly enriched in sulfur and highly enriched in oxygen as compared to WA and RA

fractions.[12, 18, 20] Compared with RA (~98.5 wt% of WA), sulfur and oxygen contents of IAA were 28 wt% and 90 wt% higher, respectively. Using ESI FT-ICR MS, Stanford et al.[11] characterized material partitioned at the interface of a water-in-diluted bitumen emulsion (diluent used was d-heptol 1:1), showing at low bitumen concentrations (high bitumen dilution), 0.1 and 0.5 wt% bitumen in d-heptol 1:1, the interfacial material was enriched in O_4 and O_3S species. The interfacial material was likely IAA, with other studies confirming the preferential adsorption of asphaltenes at high bitumen dilutions.[2, 50] It is now generally accepted that the IAA fraction is enriched in both oxygen and sulfur.[17]

The H/C ratio of RA heavy crude oil was ~1.04, while the H/C ratio for IAA was slightly higher at H/C = 1.21, suggesting preferential adsorption of more aliphatic species at the oil-water interface. Such behavior is in good agreement with the results of Sjöblom et al.[15] who extracted the most interfacially active asphaltene fraction adsorbed on calcium carbonate. Indicative of aromaticity, such differences in H/C ratio may contribute to the preferential adsorption of IAA relative to RA, resulting from the increased solubility of the more aromatic RA fraction. However, the difference in H/C ratio between RA and IAA is only one of the governing parameters to describe interfacial activity of asphaltenes.

Table 1. Elemental composition of WA, RA and IAA extracted from heavy crude oil and WA from bitumen.

Asphaltene fraction	C (wt %)	H (wt %)	N (wt %)	S (wt %)	O (wt %)	H:C	Total wt%
WA	84.53 ±1.17	7.39 ±0.39	1.29 ±0.15	3.33 ±0.63	2.53 ±0.78	1.05	99.06
RA	84.05 ±2.45	7.30 ±0.22	1.32 ±0.10	3.45 ±1.45	2.41 ±0.61	1.04	98.53
IAA	78.77 ±3.35	7.93 ±1.38	1.21 ±0.20	4.43 ±0.77	4.57 ±0.42	1.21	98.12
$WA_{bitumen}$	80.20 ±1.15	7.39 ±0.22	1.15 ±0.01	9.32 ±0.42	1.95 ±0.50	1.11	100.01

Figure 1 compares the FTIR spectra of three asphaltene fractions extracted from heavy crude oil. All FTIR spectra were normalized using the strong aliphatic C−H stretching vibration between 2780 and 3000 cm^{-1}, enabling comparison of functional groups in each asphaltene fraction. Following normalization there was no noticeable change in the C−H bending vibration between 1380 and 1460 cm^{-1} for all three fractions. The aromatic C=C stretching vibration at 1600 cm^{-1} is present in all three fractions, although the measured absorbance is greater in IAA than RA and WA. From elemental analysis, IAA is less aromatic than RA and WA. The higher absorbance of the aromatic C=C stretch in IAA may be influenced by the

strong neighbouring peak of C=O, making the peak height analysis more difficult. Coupling between these groups may also increase the electrical dipole moment, leading to greater interactions with IR radiation and thus stronger peaks. The C=O stretching vibration at 1700 cm^{-1} is lower in intensity for WA and RA than IAA, with the IAA peak shifted slightly to 1670 cm^{-1}, which may be attributed to conjugation (overlapping p orbitals) of asphaltenes in IAA, as the wavenumber of the C=O stretch is highly dependent on its proximity to aromatic rings.[51]

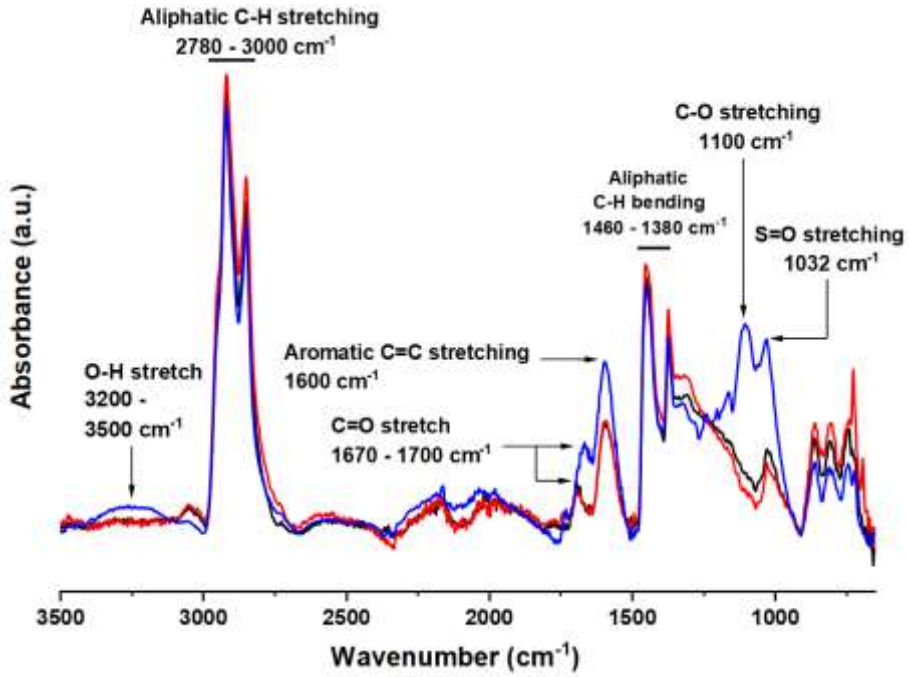

Figure 1. Normalized FTIR spectra of asphaltene fractions extracted from heavy crude oil: WA (black), RA (red) and IAA (blue).

The most significant differences in IR spectra between IAA and RA subfractions are shown by the S=O and C−O stretching vibrations at 1032 cm^{-1} and 1100 cm^{-1}, respectively. Higher S=O content of IAA supports previous findings of increased O_3S in the interfacial material,[20] while C−O and C=O also contribute to the higher oxygen content of IAA compared to RA. For the IAA fraction, a small broad peak was observed between 3000 and 3500 cm^{-1}, which is attributed to O−H stretching vibrations. While the intensity is weak, its presence may provide some evidence of contributions from O−H to the higher oxygen content in IAA. Even though all samples were dried in a vacuum oven prior to analysis, the O−H stretch may have resulted from adsorbed water by the partitioning of IAA at the oil-water interface, although a simple calculation based on the H:O ratio confirmed the retained water was likely negligible.

Small Angle Neutron Scattering

WA-type: Figure 2 compares the scattering intensity for 5 g/L WA in d-toluene extracted from bitumen (Fig. 2a) and heavy crude oil (Fig. 2b). Qualitatively, the two SANS spectra showed the same general trend in the Q-range $\geq 10^{-2}\text{Å}^{-1}$, with fits to the scattering profiles showing similar nanoaggregate size and shape for the two WA samples. The weak scattering in the low-Q region ($Q < 10^{-2}$ Å^{-1}) prevented useful comparison of the two WA samples in d-toluene, with the concentration of asphaltene clusters in d-toluene too low to produce sufficient scattering, see Fig. 3 for the low-Q scattering profile of WA heavy crude oil in d-toluene. In the Q-range $\sim 1 \times 10^{-2}$ to 2×10^{-2} Å^{-1}, the scattering intensity of WA heavy crude oil appeared to approach an asymptote at ~0.8 cm^{-1}. Such behavior was less evident from the scattering intensity of WA bitumen, indicating the likely presence of larger structures outside the Q-range studied.

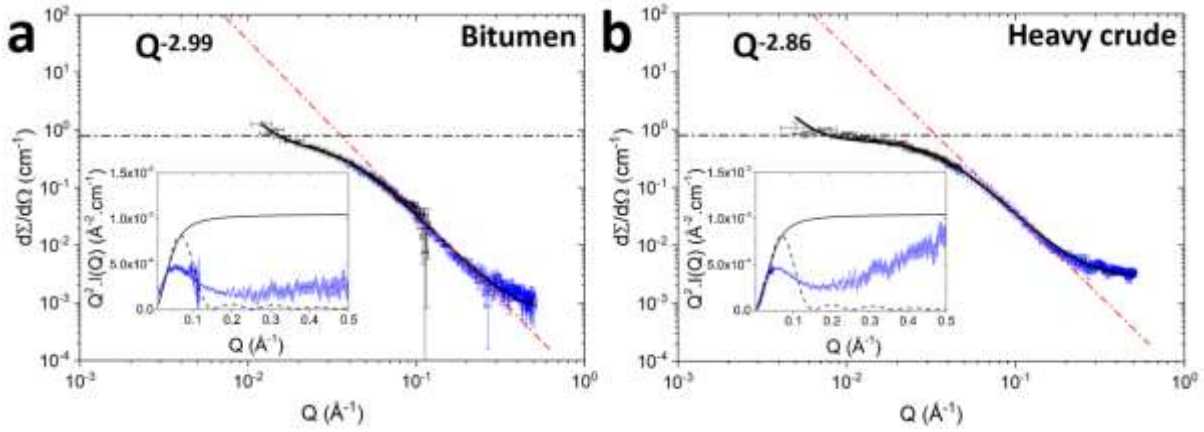

Figure 2. SANS data of 5 g/L WA in d-toluene with asphaltenes extracted from bitumen (a) and heavy crude oil (b). The solid line represents the Broad Peak model fit and insets show the corresponding Kratky plots. Theoretical curves for a homogeneous sphere (dash line) and Gaussian chain (solid line) are included in the insets as reference. Dash-dot lines in the main figures represent the slope of the Porod region (Lorentzian exponent) and the asymptote in scattering intensity for WA heavy crude oil.

Table 2. Fitting parameters of the Broad Peak model to the SANS data of 5 g/L WA in d-toluene with asphaltenes extracted from bitumen and heavy crude oil.

WA Sample	Fitting parameters					
	χ^2	Background (cm^{-1})	Porod scale	Lorentz scale (cm^{-1})	Characteristic length (Å)	Lorentzian exponent
Bitumen	2.42	0.0006	1.58×10^{-8} $\pm6.07\times10^{-10}$	0.53 ± 0.01	24.9 ± 0.2	2.99 ± 0.01
Heavy crude oil	3.17	0.0007	6.17×10^{-10} $\pm2.14\times10^{-11}$	0.65 ± 0.01	28.0 ± 0.2	2.86 ± 0.01

* χ^2 represents the reduced chi-squared value.

A summary of the Broad Peak model fitting parameters to the SANS data of both WA samples is provided in Table 2. The Broad Peak model provides an excellent fit to the SANS data of both WA samples, as confirmed by the low χ^2 values, from which the characteristic lengths were found to be similar at 24.9 and 28.0 Å for WA bitumen and WA heavy crude oil, respectively. Considering the comparable Lorentzian exponents, the two WA samples can be regarded as being physically similar in nanoaggregate size and shape. Comparing the S and O contents of WA heavy crude oil and bitumen (Table 1), it is clear that despite these differences in S and O contents, the heteroatom content does not appear to strongly influence the size and shape of the resulting nanoaggregates.

Using the Broad Peak model with the peak position set to $Q = 0$ $Å^{-1}$, the Lorentz scale (forward scattering from nanoaggregates) can be substituted for $I(0)$ in Eq. 4 to calculate the characteristic volume of the nanoaggregates. The characteristic volumes of WA bitumen and WA heavy crude oil nanoaggregates were 150 and 184 nm^3, respectively (a sample calculation to determine the characteristic volume is provided in the Supplementary Information A2), with the calculated volume expected to be within the volume of a sphere and the volume estimated by the Ornstein-Zernike approximation ($V \approx 33\xi^3$).[40, 52] The Ornstein-Zernike approximation defines the limit of Q^{-2}, which results from a very ill-defined structure and represents the limit within which the volume can be accurately calculated without additional information.[52] Using the characteristic length (ξ) as an equivalent radius, the sphere volume is determined to be 65 and 92 nm^3, and the volume estimated by the Ornstein-Zernike approximation to be 509 and 724 nm^3 for WA bitumen and WA heavy crude oil, respectively. Since the calculated volumes for both WA fractions are within the volume limits, the Broad Peak model fitting is shown to be realistic and provides certainty to the structural description of the asphaltene nanoaggregates.

The Porod scale is a measure of the specific interface, i.e. the interface to volume ratio for a given contrast, with a higher Porod scale value indicating the presence of asphaltene clusters in the solvent. The difference between the Porod scale values of WA bitumen and WA heavy crude oil in d-toluene likely result from differences in sample solubility, with WA heavy crude oil being slightly more soluble and thus the presence of larger asphaltene clusters is less. The higher Lorentz scale for WA heavy crude oil compared to WA bitumen at equivalent concentration (5 g/L) would also support a slight difference in sample solubility.

The Kratky plot describes the openness of the asphaltene structure, with a bell-shaped curve being the signature of a densely packed aggregate such as a sphere (dash line in Fig. 2 inset). Open structures being more solvated, such as unfolded chains, exhibit no characteristic peak, rather the Kratky plot plateaus with increasing Q values ($Å^{-1}$) (solid line in Fig. 2 inset). Qualitatively, WA bitumen is more densely packed than WA heavy crude oil but both nanoaggregates appear fractal-like. The slight difference in nanoaggregate structure was verified by the difference in Lorentzian exponents as well as the calculated volume of the nanoaggregates, with WA heavy crude oil ~22% larger than WA bitumen, even though the characteristic lengths vary by ~12%.

Solvent aromaticity: WA heavy crude oil was dispersed in d-toluene and 3:2 d-heptol at 5 g/L. Fitting the Broad Peak model to the mid and high-Q regions ($Q \geq 10^{-2}$ $Å^{-1}$) showed great similarity of WA heavy crude oil in both good (d-toluene) and poor (3:2 d-heptol) solvents. When accounting for the weak scattering in the low-Q range (WA in d-toluene), the Broad Peak model fitting parameters were unchanged apart from a slight reduction in the Porod scale, see Table 3, with and without low-Q region. The characteristic length of WA in d-toluene was 28.0 $Å^{-1}$, compared to a slightly smaller 26.3 $Å^{-1}$ when dispersed in 3:2 d-heptol. In addition, the slightly higher Lorentzian exponent for WA in 3:2 d-heptol suggests a more tightly packed nanoaggregate, which would be consistent with a decreased asphaltene-solvent interaction.[53]

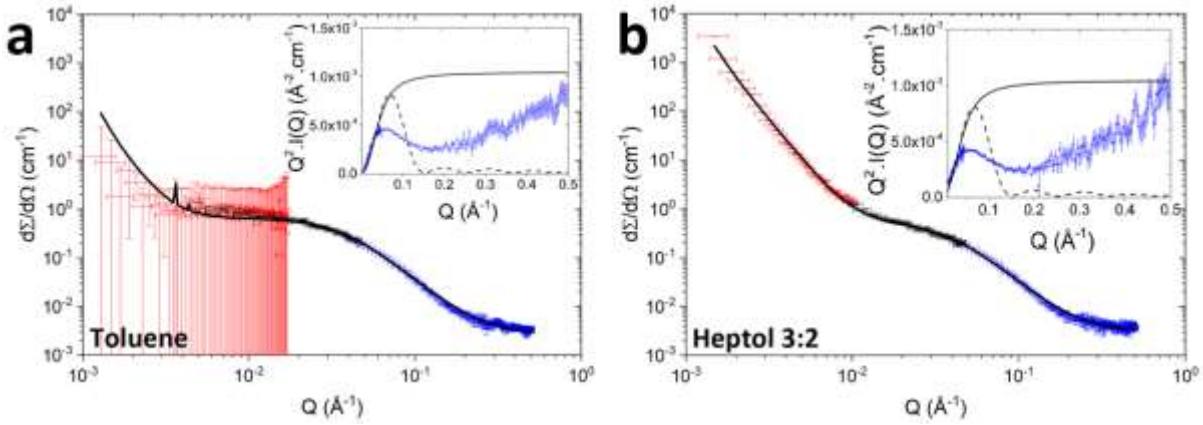

Figure 3. SANS data of WA heavy crude oil dispersed in (a) d-toluene and (b) 3:2 d-heptol at 5 g/L. SANS data fitted using the Broad Peak model is shown by the solid line. Insets show the corresponding Kratky plots and theoretical curves for a homogeneous sphere (dash line) and Gaussian chain (solid line) which are included as reference.

Table 3. Fitting parameters of the Broad Peak model to the SANS data of 5 g/L WA heavy crude oil in d-toluene (without and with low-Q data) and 3:2 d-heptol.

Sample	Fitting parameters					
	χ^2	Background (cm^{-1})	Porod scale	Lorentz scale (cm^{-1})	Characteristic length (Å)	Lorentzian exponent
Toluene (without low-Q)	3.17	0.0027	$6.17\times10^{-10} \pm 2.14\times10^{-11}$	0.65 ± 0.01	28.0 ± 0.2	2.86 ± 0.01
Toluene (with low-Q)	4.59	0.0027	$1.03\times10^{-10} \pm 1.23\times10^{-11}$	0.65 ± 0.01	28.0 ± 0.2	2.86 ± 0.01
3:2 Heptol	9.18	0.0031	$6.06\times10^{-9} \pm 1.76\times10^{-11}$	0.51 ± 0.01	26.3 ± 0.2	2.90 ± 0.02

* χ^2 represents the reduced chi-squared value.

While the characteristic lengths and Lorentzian exponents were found to be similar, the Lorentz scale factors of 0.65 cm^{-1} in d-toluene and 0.51 cm^{-1} in 3:2 d-heptol confirmed a lower asphaltenes concentration in 3:2 d-heptol. This was verified by visual assessment of the cylindrical quartz cell where WA were observed to settle in 3:2 d-heptol (Fig. S3 in Supplementary Information) but not in d-toluene. A concentration-dependent study of 1 g/L and 5 g/L WA bitumen in d-toluene (concentration-dependent change in Lorentz scale factor of 0.38), revealed similar characteristic lengths and Lorentzian exponents (Tables 2 and S1 for 5 g/L and 1 g/L, respectively), in good agreement with the study of Roux et al..[39] Hence it was reasonably assumed that the slight reduction in Lorentz scale between d-toluene and 3:2 d-heptol had a negligible effect on the data reported in Table 3, and the asphaltenes nanoaggregates in good and poor solvents were characteristically similar.

For 5 g/L WA in 3:2 d-heptol, the scattering intensity in the low-Q region ($Q < 10^{-2}$ Å^{-1}) varies inversely with the fourth power of Q, a phenomenon indicative of a sharp interface between the scattering object and solvent. This confirms the presence of large asphaltene structures, which is verified by the difference in Porod scale values, with the higher Porod scale value for WA in 3:2 d-heptol attributed to greater contrast. No Guinier regime is observed at low-Q (no intensity plateau), which means the characteristic dimension of the asphaltene clusters exceeded the probed Q-range; as Q_{min} = 0.0015 Å^{-1}, the asphaltene cluster size is larger than $2\pi/Q_{min}$ = 0.4 µm. The absence of noticeable features in the SANS data between 25 and 5000 Å would suggest there is no intermediate structure between the asphaltene nanoaggregates measured by SANS and asphaltene clusters typically measured by dynamic light scattering (DLS).[19, 54] This behaviour is in good agreement with the understanding that asphaltene nanoaggregates further aggregate to form asphaltene clusters.[6]

E-SARA fractions: Fitting the Broad Peak model to the SANS data of 5 g/L RA and IAA in d-toluene, the characteristic lengths and Lorentzian exponents for RA and IAA were 28.8 and 59.7 Å and 2.86 and 2.20, respectively (Table 4), confirming a significant difference between the nanoaggregate structures of RA and IAA.

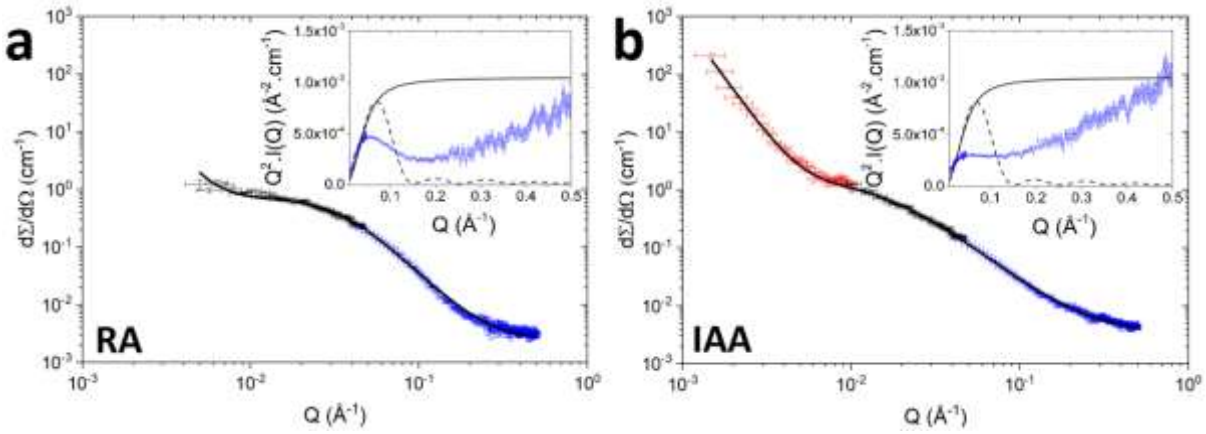

Figure 4. SANS data of 5 g/L RA in d-toluene (a) and 5 g/L IAA in d-toluene (b). SANS data fitted using the Broad Peak model is shown by the solid line. Insets show the corresponding Kratky plots and theoretical curves for a homogenous sphere (dash line) and Gaussian chain (solid line) which are included as reference.

Table 4. Fitting parameters of the Broad Peak model to the SANS data of 5 g/L RA and IAA in d-toluene with asphaltenes extracted from heavy crude oil.

Sample	Fitting parameters					
	χ^2	Background (cm^{-1})	Porod scale	Lorentz scale (cm^{-1})	Characteristic length (Å)	Lorentzian exponent
RA	3.61	0.0024	7.80×10^{-10} $\pm6.92\times10^{-11}$	0.70 ± 0.01	28.8 ± 0.2	2.86 ± 0.01
IAA	1.62	0.0036	8.59×10^{-10} $\pm1.61\times10^{-11}$	1.33 ± 0.03	59.7 ± 0.9	2.20 ± 0.01

* χ^2 represents the reduced chi-squared value.

The smaller Lorentzian exponent of IAA, 2.2 compared with 2.9 for RA, confirms the IAA nanoaggregates are less dense (more porous structures). Differences in nanoaggregate structures can also be qualitatively assessed by comparing the blue profile shown in the Kratky plots, with the RA fraction exhibiting a more prominent peak in the Q-range 0 – 0.1 $Å^{-1}$, which is indicative of a compact structure, and for IAA, the Kratky plot features a high-Q upturn from a plateau, which is more representative of a Gaussian chain.[46] Commonly, the Flory mean field theory of polymers describes the structure as self-attracting chains (Lorentzian exponent = 3), random-walk chains (Lorentzian exponent = 2) and swollen chains (Lorentzian exponent = 1.67), dependent on the solvent-solvent, monomer-monomer and solvent-monomer interactions. Based on these descriptions, the RA fraction may be described as a self-attracting chain and the IAA fraction a random-walk chain. However, a Lorentzian exponent of 2 can also infer scattering from thin disk structures. When fitted using a core-shell cylinder model, a length (disk height) value close to zero was obtained which is considered unrealistic, and from the fit of the shape-dependent model, the χ^2 value was 20, significantly larger than the χ^2 values of the shape-independent model reported in Table 4, hence the disk-like structure for IAA was disregarded.

An additional factor which can result in a Lorentzian exponent of 2 is scattering from ill-defined structures of varying size and shape.[40] This is highlighted when the calculated volume of the nanoaggregates is not bound by the volumes of a sphere or that estimated by the Ornstein-Zernike approximation. For RA, the calculated volume from the Lorentz scale was 197 nm^3 and falls within the volumes estimated for a sphere (100 nm^3) and the Ornstein-Zernike approximation (788 nm^3). However, the calculated volume of IAA was 376 nm^3 and falls outside the range estimated for a sphere (891 nm^3) and the Ornstein-Zernike approximation (7022 nm^3). To satisfy the volume criteria, the asphaltene volume fraction (Φ) as described in

Eq. 4 should be decreased to < 20% of the initial asphaltene volume fraction. Since this sample was not observed to form asphaltene precipitates, such a large discrepancy in Φ is unlikely to be realistic. The calculation assumes a constant SLD between asphaltene types, and although this would likely differ between RA and IAA, it is unlikely to account for such a significant shift in the Lorentz scale, despite being proportional to the square of the difference in SLD. Therefore the smaller Lorentzian exponent of IAA can be attributed to scattering from nanoaggregates of increased polydispersity and randomness of structures, both in size and shape.

Nanostructure-assisted laser desorption/ionization (NALDI) analysis of the two asphaltene sub-fractions dispersed in toluene at 50 g/L revealed an increased polydispersity of the IAA fraction. Figure 5 shows the full NALDI data for RA and IAA at 25°C. The molecular weight of RA spanned the approximate range 200 to 1400 Da with a peak intensity in the region of 400 Da. For IAA a clear bimodal distribution was observed. The molecular weight of IAA spanned the full range of the NALDI measurement, with two peak intensities in the regions of 400 Da and 1200 Da. The bimodal distribution of IAA reflects at least two asphaltene sizes with the smaller and larger sizes likely representing asphaltene molecules and aggregates. The NALDI data is in good agreement with the SANS data, and the Lorentzian exponent of 2 is likely attributed to the increased polydispersity and randomness of IAA nanoaggregate structures.

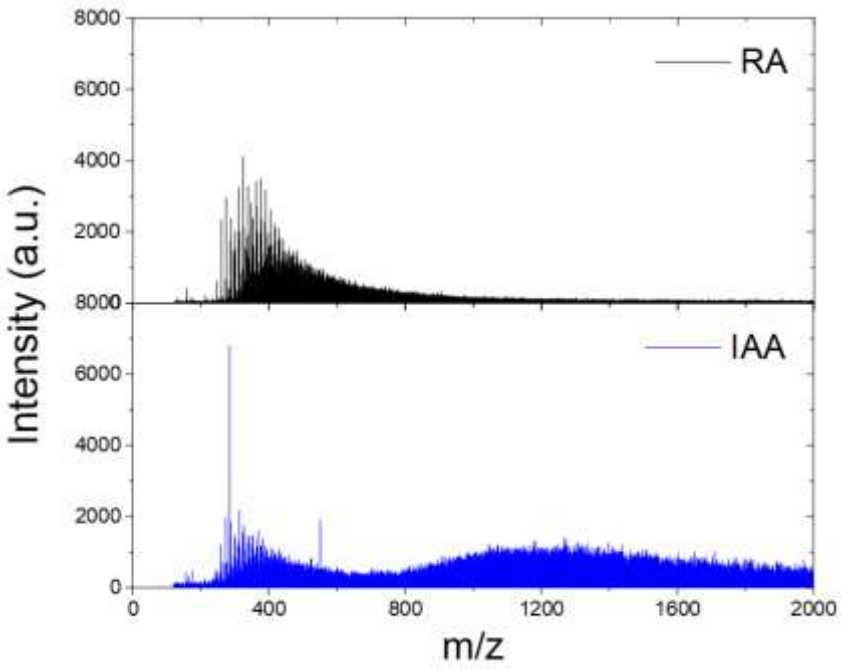

Figure 5. Molecular weight distribution of RA and IAA fractions measured using NALDI.

The Broad Peak model offers several advantages when fitting SANS data of complex systems. However, the model is biased towards larger structures with the scattering intensity weighted to the sixth power of the particle radius.[55] The model, therefore, has a strong correlation between the object volume and scattering intensity, and hence for IAA the SANS profile may be influenced by structures of the higher Mw species. This larger fraction is clearly seen in the IAA fraction by the scattering intensity increase in the low-Q region ($Q < 10^{-2}$ Å^{-1}) and confirms the presence of asphaltene clusters. However, asphaltene clusters were also observed for 5 g/L WA in 3:2 d-heptol but the nanoaggregate structure was similar to WA in d-toluene which showed few asphaltene clusters.

The current study confirms the physical characteristics of IAA and RA nanoaggregates to be inconsistent. While differences in elemental composition did not significantly influence nanoaggregates formed from WA extracted from bitumen and heavy crude oil (Table 2), the significant variation in nanoaggregate structure between RA and IAA likely results from differences in key functional groups (S=O and C−O) and possibly the location of these functional groups within the asphaltene structure. These structural features appear to govern the asphaltene-asphaltene interactions which led to significantly different asphaltene nanoaggregate structures.

The nanoaggregate size and shape data, coupled with the apparent dependence on asphaltenes functional groups, suggests aggregation via $\pi - \pi$ interactions is not fully descriptive of the SANS data, and aggregation likely includes other mechanisms, such as those described by the supramolecular model. These findings are important because the aggregation mechanism is fundamental to problems associated with asphaltenes precipitation and fouling, and will help guide new thinking when designing effective dispersants to treat both RA and IAA fractions.

CONCLUSION

Small angle neutron scattering was used to study the size and shape of i) whole asphaltenes (WA) extracted from bitumen and heavy crude oil; and ii) interfacially active asphaltenes (IAA) and remaining asphaltenes (RA) separated by E-SARA fractionation of WA heavy crude oil. The size and shape of WA nanoaggregates was shown to be insensitive to oil type, even

though the sulfur (S) and oxygen (O) contents of the two WAs (extracted from heavy crude oil and bitumen) varied substantially; as well as solvent aromaticity (WA heavy crude oil), even though the poorer solvent (3:2 d-heptol) led to the formation of larger asphaltene clusters. For IAA and RA fractionated from WA heavy crude oil, a significant difference in the SANS data was observed. Fitting the shape-independent Broad Peak model to the SANS data, the characteristic lengths and Lorentzian exponents for RA and IAA were found to be 29 and 60 Å and 2.9 and 2.2, respectively, indicating the RA nanoaggregates were smaller than IAA nanoaggregates, and IAA nanoaggregates were less compact compared to RA nanoaggregates.

Although the IAA and RA fractions had differences in S and O content (IAA_S = 4.43 wt%, IAA_O = 4.57 wt%, RA_S = 3.45 wt%, RA_O = 2.41 wt%), similar differences in elemental composition were not found to influence the size and shape of WA nanoaggregates extracted from bitumen and heavy crude oil. Therefore, this study highlighted that the asphaltenes functional groups, particularly S=O and $C-O$ species, strongly affect the aggregation mechanism(s) and resultant nanoaggregate structures (size and shape), with aggregation behavior more consistent with the supramolecular growth model.

ASSOCIATED CONTENT

Supplementary Information

The Supplementary Information is available free of charge on

SANS data DOI: 10.5291/ILL-DATA.9-10-1531.[56]

A1. Scattering Length Density, Figure S1. Average SLD of WA extracted from heavy crude oil; **A2. Calculating nanoaggregate volume** (WA heavy crude oil); **A3. 1 g/L WA in d-toluene SANS, Figure S2.** SANS spectra of 1 g/L WA in d-toluene extracted from bitumen. The solid line represents the Broad Peak model fit; **Table S1.** Fitting parameters of the Broad Peak model to the SANS profile of 1 g/L WA in d-toluene extracted from bitumen; **A4. Asphaltene precipitation in 3:2 d-heptol. Figure S3.** Image of SANS cylindrical quartz cell of 5 g/L WA in 3:2 d-heptol after a 6 h test. A small accumulation of precipitated asphaltenes was observed at the cell base. This is confirmed by the changing color intensity along the

highlighted line in the main image. Low color intensity (15 a.u.) corresponds to region of precipitated asphaltenes.

AUTHOR INFORMATION

Corresponding author

*Email: D.Harbottle@leeds.ac.uk

Notes

The authors declare no competing financial interest.

ACKNOWLEDGMENTS

This research was completed at the Engineering and Physical Sciences Research Council (EPSRC) Centre for Doctoral Training in Complex Particulate Products and Processes (EP/L015285/1), in collaboration with Infineum UK Ltd., who we greatly acknowledge for their support of this work. Z.X. acknowledges funding from the Natural Sciences and Engineering Research Council (NSERC) – Industrial Research Chair (IRC) Program in Oil Sands Engineering. D.H. acknowledges funding from the Royal Academy of Engineering Industry-Academia Partnership Program (IAPP1/100150). This work benefited from the use of the SasView application, originally developed under NSF award DMR-0520547. SasView contains code developed with funding from the European Union's Horizon 2020 research and innovation program under the SINE2020 project, grant agreement No 654000. The authors would also like to thank Ms Jing Zheng from the Mass Spectrometry Facility, Department of Chemistry, University of Alberta, for conducting the NALDI tests.

REFERENCES

1. Harbottle, D.; Chen, Q.; Moorthy, K.; Wang, L.; Xu, S.; Liu, Q.; Sjoblom, J.; Xu, Z., Problematic Stabilizing Films in Petroleum Emulsions: Shear Rheological Response of Viscoelastic Asphaltene Films and the Effect on Drop Coalescence. *Langmuir* **2014,** *30* (23), 6730-6738.
2. Wu, X., Investigating the Stability Mechanism of Water-in-Diluted Bitumen Emulsions through Isolation and Characterization of the Stabilizing Materials at the Interface. *Energy & Fuels* **2003,** *17* (1), 179-190.
3. Rane, J. P.; Harbottle, D.; Pauchard, V.; Couzis, A.; Banerjee, S., Adsorption kinetics of asphaltenes at the oil–water interface and nanoaggregation in the bulk. *Langmuir* **2012,** *28* (26), 9986-9995.
4. Wang, S.; Segin, N.; Wang, K.; Masliyah, J. H.; Xu, Z., Wettability Control Mechanism of Highly Contaminated Hydrophilic Silica/Alumina Surfaces by Ethyl Cellulose. *The Journal of Physical Chemistry C* **2011,** *115* (21), 10576-10587.
5. Natarajan, A.; Kuznicki, N.; Harbottle, D.; Masliyah, J.; Zeng, H.; Xu, Z., Understanding Mechanisms of Asphaltene Adsorption from Organic Solvent on Mica. *Langmuir* **2014,** *30* (31), 9370-9377.
6. Mullins, O. C., The Asphaltenes. *Annual Review of Analytical Chemistry* **2011,** *4* (1), 393-418.
7. Speight, J. G., Petroleum Asphaltenes - Part 1: Asphaltenes, Resins and the Structure of Petroleum. *Oil & Gas Science and Technology - Rev. IFP* **2004,** *59* (5), 467-477.
8. Hoepfner, M. P.; Fogler, H. S., Multiscale Scattering Investigations of Asphaltene Cluster Breakup, Nanoaggregate Dissociation, and Molecular Ordering. *Langmuir* **2013,** *29* (49), 15423-15432.

9. Wang, H.; Xu, H.; Jia, W.; Liu, J.; Ren, S., Revealing the Intermolecular Interactions of Asphaltene Dimers by Quantum Chemical Calculations. *Energy & Fuels* **2017,** *31* (3), 2488-2495.
10. Stanford, L. A.; Rodgers, R. P.; Marshall, A. G.; Czarnecki, J.; Wu, X. A.; Taylor, S., Detailed Elemental Compositions of Emulsion Interfacial Material versus Parent Oil for Nine Geographically Distinct Light, Medium, and Heavy Crude Oils, Detected by Negative- and Positive-Ion Electrospray Ionization Fourier Transform Ion Cyclotron Resonance Mass Spectrometry. *Energy & Fuels* **2007,** *21* (2), 973-981.
11. Stanford, L. A.; Rodgers, R. P.; Marshall, A. G.; Czarnecki, J.; Wu, X. A., Compositional Characterization of Bitumen/Water Emulsion Films by Negative- and Positive-Ion Electrospray Ionization and Field Desorption/Ionization Fourier Transform Ion Cyclotron Resonance Mass Spectrometry. *Energy & Fuels* **2007,** *21* (2), 963-972.
12. Yang, F.; Tchoukov, P.; Pensini, E.; Dabros, T.; Czarnecki, J.; Masliyah, J.; Xu, Z., Asphaltene Subfractions Responsible for Stabilizing Water-in-Crude Oil Emulsions. Part 1: Interfacial Behaviors. *Energy & Fuels* **2014,** *28* (11), 6897–6904.
13. Clingenpeel, A. C.; Rowland, S. M.; Corilo, Y. E.; Zito, P.; Rodgers, R. P., Fractionation of Interfacial Material Reveals a Continuum of Acidic Species That Contribute to Stable Emulsion Formation. *Energy & Fuels* **2017,** *31* (6), 5933-5939.
14. Jarvis, J. M.; Robbins, W. K.; Corilo, Y. E.; Rodgers, R. P., Novel Method To Isolate Interfacial Material. *Energy & Fuels* **2015,** *29* (11), 7058-7064.
15. Subramanian, S.; Simon, S.; Gao, B.; Sjöblom, J., Asphaltene fractionation based on adsorption onto calcium carbonate: Part 1. Characterization of sub-fractions and QCM-D measurements. *Colloids and Surfaces A: Physicochemical and Engineering Aspects* **2016,** *495* (Supplement C), 136-148.
16. Subramanian, S.; Sørland, G. H.; Simon, S.; Xu, Z.; Sjöblom, J., Asphaltene fractionation based on adsorption onto calcium carbonate: Part 2. Self-association and aggregation properties. *Colloids and Surfaces A: Physicochemical and Engineering Aspects* **2017,** *514*, 79-90.
17. Qiao, P.; Harbottle, D.; Tchoukov, P.; Masliyah, J.; Sjoblom, J.; Liu, Q.; Xu, Z., Fractionation of Asphaltenes in Understanding Their Role in Petroleum Emulsion Stability and Fouling. *Energy & Fuels* **2017,** *31* (4), 3330–3337.
18. Yang, F.; Tchoukov, P.; Dettman, H.; Teklebrhan, R. B.; Liu, L.; Dabros, T.; Czarnecki, J.; Masliyah, J.; Xu, Z., Asphaltene Subfractions Responsible for Stabilizing Water-in-Crude Oil Emulsions. Part 2: Molecular Representations and Molecular Dynamics Simulations. *Energy & Fuels* **2015,** *29* (8), 4783-4794.
19. Qiao, P.; Harbottle, D.; Li, Z.; Tang, Y.; Xu, Z., Interactions of Asphaltene Subfractions in Organic Media of Varying Aromaticity. *Energy & Fuels* **2018,** *32* (10), 10478-10485.
20. Qiao, P.; Harbottle, D.; Tchoukov, P.; Wang, X.; Xu, Z., Asphaltene Subfractions Responsible for Stabilizing Water-in-Crude Oil Emulsions. Part 3. Effect of Solvent Aromaticity. *Energy & Fuels* **2017,** *31* (9), 9179–9187.
21. Mullins, O. C.; Sabbah, H.; Eyssautier, J.; Pomerantz, A. E.; Barré, L.; Andrews, A. B.; Ruiz-Morales, Y.; Mostowfi, F.; McFarlane, R.; Goual, L.; Lepkowicz, R.; Cooper, T.; Orbulescu, J.; Leblanc, R. M.; Edwards, J.; Zare, R. N., Advances in Asphaltene Science and the Yen–Mullins Model. *Energy & Fuels* **2012,** *26* (7), 3986-4003.
22. Gray, M. R.; Tykwinski, R. R.; Stryker, J. M.; Tan, X., Supramolecular Assembly Model for Aggregation of Petroleum Asphaltenes. *Energy & Fuels* **2011,** *25* (7), 3125-3134.
23. Agrawala, M.; Yarranton, H. W., An Asphaltene Association Model Analogous to Linear Polymerization. *Industrial & Engineering Chemistry Research* **2001,** *40* (21), 4664-4672.
24. Sheu, E. Y.; Liang, K. S.; Sinha, S. K.; Overfield, R. E., Polydispersity analysis of asphaltene solutions in toluene. *Journal of Colloid and Interface Science* **1992,** *153* (2), 399-410.
25. Eyssautier, J.; Levitz, P.; Espinat, D.; Jestin, J.; Gummel, J.; Grillo, I.; Barre, L., Insight into asphaltene nanoaggregate structure inferred by small angle neutron and X-ray scattering. *The journal of physical chemistry. B* **2011,** *115* (21), 6827-37.
26. Bardon, C.; Barre, L.; Espinat, D.; Guille, V.; Li, M. H.; Lambard, J.; Ravey, J. C.; Rosenberg, E.; Zemb, T., The colloidal structure of crude oils and suspensions of asphaltenes and resins. *Fuel Science and Technology International* **1996,** *14* (1-2), 203-242.
27. Storm, D. A.; Sheu, E. Y., Characterization of colloidal asphaltenic particles in heavy oil. *Fuel* **1995,** *74* (8), 1140-1145.
28. Tanaka, R.; Hunt, J. E.; Winans, R. E.; Thiyagarajan, P.; Sato, S.; Takanohashi, T., Aggregates Structure Analysis of Petroleum Asphaltenes with Small-Angle Neutron Scattering. *Energy & Fuels* **2003,** *17* (1), 127-134.
29. Gawrys, K. L.; Kilpatrick, P. K., Asphaltenic aggregates are polydisperse oblate cylinders. *J. Colloid Interface Sci.* **2005,** *288* (2), 325-34.
30. Porte, G.; Zhou, H.; Lazzeri, V., Reversible Description of Asphaltene Colloidal Association and Precipitation. *Langmuir* **2003,** *19* (1), 40-47.

31. Headen, T. F.; Boek, E. S.; Stellbrink, J.; Scheven, U. M., Small Angle Neutron Scattering (SANS and V-SANS) Study of Asphaltene Aggregates in Crude Oil. *Langmuir* **2009,** *25* (1), 422-428.
32. McKenna, A. M.; Marshall, A. G.; Rodgers, R. P., Heavy Petroleum Composition. 4. Asphaltene Compositional Space. *Energy & Fuels* **2013,** *27* (3), 1257-1267.
33. Hoepfner, M. P.; Vilas Bôas Fávero, C.; Haji-Akbari, N.; Fogler, H. S., The Fractal Aggregation of Asphaltenes. *Langmuir* **2013,** *29* (28), 8799-8808.
34. Gawrys, K. L.; Blankenship, G. A.; Kilpatrick, P. K., On the Distribution of Chemical Properties and Aggregation of Solubility Fractions in Asphaltenes. *Energy & Fuels* **2006,** *20* (2), 705-714.
35. Spiecker, P. M.; Gawrys, K. L.; Kilpatrick, P. K., Aggregation and solubility behavior of asphaltenes and their subfractions. *J. Colloid Interface Sci.* **2003,** *267* (1), 178-93.
36. Long, B.; Chodakowski, M.; Shaw, J. M., Impact of Liquid–Vapor to Liquid–Liquid–Vapor Phase Transitions on Asphaltene-Rich Nanoaggregate Behavior in Athabasca Vacuum Residue + Pentane Mixtures. *Energy & Fuels* **2013,** *27* (4), 1779-1790.
37. Fenistein, D.; Barré, L.; Broseta, D.; Espinat, D.; Livet, A.; Roux, J.-N.; Scarsella, M., Viscosimetric and Neutron Scattering Study of Asphaltene Aggregates in Mixed Toluene/Heptane Solvents. *Langmuir* **1998,** *14* (5), 1013-1020.
38. Barré, L.; Jestin, J.; Morisset, A.; Palermo, T.; Simon, S., Relation between Nanoscale Structure of Asphaltene Aggregates and their Macroscopic Solution Properties. *Oil & Gas Science and Technology* **2009,** *64* (5), 617-628.
39. Roux, J.-N.; Broseta, D.; Demé, B., SANS study of asphaltene aggregation: concentration and solvent quality effects. *Langmuir* **2001,** *17* (16), 5085-5092.
40. Schöttl, S.; Lopian, T.; Prévost, S.; Touraud, D.; Grillo, I.; Diat, O.; Zemb, T.; Horinek, D., Combined molecular dynamics (MD) and small angle scattering (SAS) analysis of organization on a nanometer-scale in ternary solvent solutions containing a hydrotrope. *Journal of Colloid and Interface Science* **2019,** *540*, 623-633.
41. Minale, M.; Merola, M. C.; Carotenuto, C., Effect of solvents on the microstructure aggregation of a heavy crude oil. *Fuel Process. Technol.* **2018,** *177*, 299-308.
42. Yang, Y.; Chaisoontornyotin, W.; Hoepfner, M. P., Structure of Asphaltenes during Precipitation Investigated by Ultra-Small-Angle X-ray Scattering. *Langmuir* **2018,** *34* (35), 10371-10380.
43. Zeng, H.; Song, Y.-Q.; Johnson, D. L.; Mullins, O. C., Critical Nanoaggregate Concentration of Asphaltenes by Direct-Current (DC) Electrical Conductivity. *Energy & Fuels* **2009,** *23* (3), 1201-1208.
44. Espinat, D.; Fenistein, D.; Barré, L.; Frot, D.; Briolant, Y., Effects of Temperature and Pressure on Asphaltenes Agglomeration in Toluene. A Light, X-ray, and Neutron Scattering Investigation. *Energy & Fuels - ENERG FUEL* **2004,** *18*.
45. Jestin, J.; Simon, S.; Zupancic, L.; Barré, L., A Small Angle Neutron Scattering Study of the Adsorbed Asphaltene Layer in Water-in-Hydrocarbon Emulsions: Structural Description Related to Stability. *Langmuir* **2007,** *23* (21), 10471-10478.
46. Hammouda, B. Probing nanoscale structures - The SANS toolbox. https://www.ncnr.nist.gov/staff/hammouda/the_SANS_toolbox.pdf (accessed 27 July).
47. SasView SasView for Small Angle Scattering Analysis. http://www.sasview.org/ (accessed 27 June).
48. Marquardt, D. W., An Algorithm for Least-Squares Estimation of Nonlinear Parameters. *Journal of the Society for Industrial and Applied Mathematics* **1963,** *11* (2), 431-441.
49. Hammouda, B., A new Guinier-Porod model. *Journal of Applied Crystallography* **2010,** *43* (4), 716-719.
50. Xu, Y.; Dabros, T.; Hamza, H.; Shefantook, W., Destabilization of water in bitumen emulsion by washing with water. *Petroleum Science and Technology* **1999,** *17* (9-10), 1051-1070.
51. Ravikumar, C.; Hubert Joe, I.; Sajan, D., Vibrational contributions to the second-order nonlinear optical properties of π-conjugated structure acetoacetanilide. *Chemical Physics* **2010,** *369* (1), 1-7.
52. Ornstein, L. S. a. Z., F., Accidental deviations of density and opalescence at the critical point of a single substance. *Royal Netherlands Academy of Arts and Sciences, Amsterdam* **1914,** *17*, 793-806.
53. Wang, S.; Liu, J.; Zhang, L.; Masliyah, J.; Xu, Z., Interaction forces between asphaltene surfaces in organic solvents. *Langmuir* **2009,** *26* (1), 183-190.
54. Burya, Y. G.; Yudin, I. K.; Dechabo, V. A.; Kosov, V. I.; Anisimov, M. A., Light-scattering study of petroleum asphaltene aggregation. *Appl. Opt.* **2001,** *40* (24), 4028-4035.
55. Beaucage, G.; Kammler, H. K.; Pratsinis, S. E., Particle size distributions from small-angle scattering using global scattering functions. *Journal of Applied Crystallography* **2004,** *37* (4), 523-535.
56. Dowding, P.; Ballard, D. A.; Cattoz, B.; Grillo, I.; Harbottle, D.; Porcar, L.; Prevost, S.; Pugejs, A.; Qiao, P.; Willis, C.; Yan, C., Investigating the Structure and Stabilisation Mechanism of Asphaltene Subfractions. *Institut Laue-Langevin (ILL): Grenoble* **2018**.